Available online at www.sciencedirect.com

ScienceDirect

Procedia Structural Integrity 2 (2016) 166–173

Structural Integrity Procedia

www.elsevier.com/locate/procedia

21st European Conference on Fracture, ECF21, 20-24 June 2016, Catania, Italy

Modelling mixed-mode fracture in poly(methylmethacrylate) using peridynamics

Francesco Caimmi[a,]*, Elyas Haddadi[b,c], Naghdali Choupani[b,c], Claudia Marano[a], Luca Andena[a]

[a]*Chemistry, Materials and Chemical Engineering Department "Giulio Natta", Politecnico di Milano, P.za Leonardo da Vinci 32, I-20133 Milano, Italy*

[b]*Faculty of Mechanical Engineering, Sahand University of Technology,Sahand NewTown,51335-1996, Tabriz, Iran*

[c]*Institute of Polymeric Materials, Sahand University of Technology, Sahand NewTown,51335-1996,Tabriz, Iran*

Abstract

Peridynamics (Silling (2000)) is a non-local continuum theory that is particularly suited to handle discontinuities in the displacement field, such as those arising during fracture. Peridynamics prescribes that each material point interacts with all its neighbors contained in a sphere of given radius; this assumption introduces a characteristic length scale in the continuum description. In a nutshell, the interactions between material points depend on their relative distance; in the peridynamics framework this distance is called the “bond length”. The equations of motion, holding at each material point, link the material point acceleration to the integral over the point neighborhood of a force density field, whose strength depend on bond-stretches, i.e. the ratio of the actual bond-length over the initial one. In these equations the displacement gradient does not appear, thus naturally allowing for discontinuities in the displacement field to occur. As to failure, the simplest possible damage description is provided by an interaction law prescribing the force to vanish when a critical bond-stretch threshold is crossed; this parameter can be related to the Mode I critical strain energy release rate. A single parameter is needed to describe failure, in principle under every possible loading condition.

In this work the predictive abilities of peridynamics were checked against experimental results in the case of mixed-mode failure of brittle polymers. Pre-cracked poly(methylmethacrylate) (PMMA) samples were tested using different specimens, in order to obtain Mode I, Mixed-Mode and Mode II loading conditions. The material was assumed to behave according to a peridynamics brittle elastic material model; the parameters needed to calibrate the elastic behavior were determined from Mode I tests, as was the critical stretch.The peridynamics simulations of mixed-mode tests were able to catch the correct fracture initiation load and to provide a fair description of the crack path under different conditions. The peridynamics model was also able to qualitatively capture the typical “nail” shape assumed by the crack front during propagation.

Peer-review under responsibility of the Scientific Committee of PCF 2016.

* Corresponding author. Tel.: +39.02.2399.4711; fax: +39.02.7063.8173.
E-mail address: francesco.caimmi@polimi.it,

Peer review under responsibility of the Scientific Committee of PCF 2016.
10.1016/j.prostr.2016.06.022

Peer-review under responsibility of the Scientific Committee of ECF21.

Keywords: peridynamics; PMMA; mixed-mode fracture

1. Introduction

Peridynamics is a non-local theory that describes the mechanical behavior of continua; it was originally introduced by Silling (2000) with the explicit objective of tackling fracture problems. The primary feature allowing peridynamics to deal with the nucleation and the evolutions of cracks, and generally with discontinuous displacement fields, is its representation of the equation of motion in an integro-differential form rather than by the partial differential equation form which is common in classical continuum theories. Using such a formulation the constraints on the smoothness of the displacement field which are typical of the classical continuum models can be significantly relaxed, as long as the integral appearing in the motion equations (see Sec.2) can be evaluated. The non-local character of peridynamics arises from the fact that each material point (sometimes called a "particle" in peridynamics) is allowed interacting, via a force field, with all the other material points within a given distance; the latter is called the horizon and is assumed to be a material property. This formulation allows dealing with problems involving an intrinsic length scale.

Different peridynamics formulations are available; they differ mostly for the type of interactions that are allowed between material points. In the so called bond-based formulation, see Silling (2000), the material points interact in a pairwise fashion as if they were connected by a spring network; the force exchanged between two particles is always directed as the line joining the material points themselves. Bond-based formulations are somewhat limited and to overcome their limitations the so called state-based formulations were introduced by Silling et al. (2007); in these formulations the force exchanged by two particles depends on the collective deformation of the material inside the horizon of a given material particle.

The first peridynamics models were initially developed for homogenous isotropic elastic materials but nowadays there are peridynamics constitutive models to mimic the behavior of fiber reinforced composites (see for example Oterkus and Madenci (2012)), of plastic (Mitchell (2011)) and of viscoplastic materials (Foster et al. (2010)); it has been shown that classical material models can be used within the peridynamics framework following a standard adaptation procedure (see Silling et al. (2007) for a thorough discussion of this issue). Initially developed only to model the mechanical behavior of continua, peridynamics has been extended to include the thermal behavior (see Madenci and Oterkus (2013) for a discussion) and also to be used in multiphysics settings, as for example in the work by Oterkus et al. (2013).

Irrespective of the material model used, peridynamics easily allows a representation of cracks initiation and propagation by adding a fracture criterion, which is usually specified as a critical event that suppresses the interactions between neighboring material points. The most commonly used criteria are strain based, similarly to what was proposed by Silling and Askari (2005) for their bond-based formulation, and usually depend on single parameter. Peridynamics has been applied to model failure in engineering applications: for instance, it was used to model failure of concrete slabs under impact, to study crack branching under dynamic conditions by Ha and Bobaru (2010) and to study the failure of microelectronics packaging by Agwai et al. (2008). However, most of the technical literature deals with the development of material models and with the development of numerical techniques to solve peridynamics problems—which are very important as the complexity of peridynamics equations makes analytical solutions nearly impossible to find—and relatively little attention has been devoted to the quantitative evaluation of the predictive capabilities of peridynamics fracture models. Madenci and Oterkus (2013, chapter 6) checked the predictions of a simple failure model against the data generated with the mixed mode specimen proposed by Ayatollahi and Aliha (2009), finding fair agreement as to the fracture load and a good agreement with respect to the predicted fracture paths.

To contribute to the validation of peridynamics predictions, in this work we use peridynamics to model failure of PMMA using different specimens to generate different mixed mode conditions; after a brief review of the basics of

peridynamics is given in Sec. 2, Sec. 3 describes the experimental tests that were run for this research and the numerical models used to simulate them. Results are presented in Sec. 4. Sec. 5 presents some closing remarks.

2. Peridynamics background

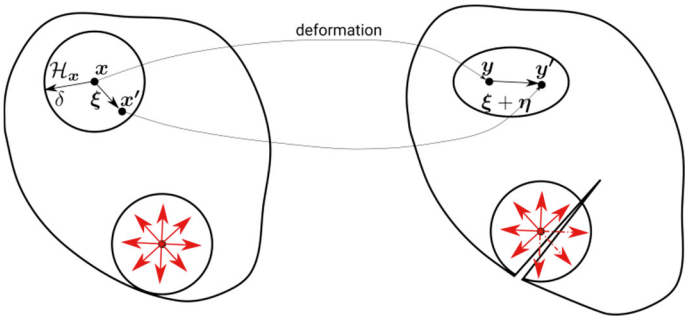

Figure 1. Motion of peridynamics solid. The motion can cause a crack to appear where no crack was initially present.

Referring to Figure 1, peridynamics assumes that a material point placed at $\boldsymbol{x}$ interacts with all the points that are inside a sphere of radius δ, called the horizon. The spherical region centered at $\boldsymbol{x}$ is called the family of $\boldsymbol{x}$ and is denoted by $\mathcal{H}_{\boldsymbol{x}}$. Peridynamics postulates the following equation of motion for each point $\boldsymbol{x}$:

$$\rho\ddot{\boldsymbol{u}} = \int_{\mathcal{H}_x} \boldsymbol{f}(\boldsymbol{u}'-\boldsymbol{u}, \boldsymbol{x}'-\boldsymbol{x}) dV' + \boldsymbol{b}, \tag{1}$$

where $\boldsymbol{u}$ is the displacement field, $\boldsymbol{b}$ is a body force vector and $\boldsymbol{f}$ is a vector valued function expressing the force (per unit volume squared) exerted on point $\boldsymbol{x}$ by a point $\boldsymbol{x}'$ in its family. Let $\boldsymbol{y}$ and $\boldsymbol{y}'$ denote the position occupied after motion by $\boldsymbol{x}$ and $\boldsymbol{x}'$ respectively, and denote the distance in the reference configuration between two points as $\boldsymbol{\xi} = \boldsymbol{x}' - \boldsymbol{x}$; finally, let the relative displacement be denoted by $\boldsymbol{\eta} = \boldsymbol{u}' - \boldsymbol{u}$. Although stress-like quantities can be evaluated in peridynamics (see Silling et al. (2007)), there is no true analogous concept appearing in the peridynamics equation, the interactions being completely characterized by the force field $\boldsymbol{f}$.

In this work, state-based peridynamics was used, as it will be briefly outlined in what follows; for a full description the reader is referred to the work by Silling et al. (2007). In a nutshell, states are operators acting on vectors in the family of some point; a vector state is a state whose image is itself a vector. A central role in peridynamics is played by the force state $\bar{\boldsymbol{T}}[\boldsymbol{x}, t] < \boldsymbol{x}' - \boldsymbol{x} >$; the bar is used to denote states and the notation adopted means that the state depends on the arguments between square brackets and acts on the bond between angular brackets. The various brackets will be omitted when no ambiguity may rise. Using states Eq. 1 is recast in the following form:

$$\rho\ddot{\boldsymbol{u}} = \int_{\mathcal{H}_x} \{\bar{\boldsymbol{T}}[\boldsymbol{x}, t] < \boldsymbol{x}' - \boldsymbol{x} > - \bar{\boldsymbol{T}}[\boldsymbol{x}', t] < \boldsymbol{x} - \boldsymbol{x}' >\} dV' + \boldsymbol{b}, \tag{2}$$

where the force density is now expressed in terms of the difference of force states.

For the so called ordinary materials, the force state is expressed as $\bar{\boldsymbol{T}} = \bar{t}\,\bar{\boldsymbol{M}}$, where $\bar{\boldsymbol{M}}$ is the deformed direction vector state, given by $\bar{\boldsymbol{M}} = \boldsymbol{\xi} + \boldsymbol{\eta} / \left\| \boldsymbol{\xi} + \boldsymbol{\eta} \right\|$ and $\bar{t}$ is a scalar state called the scalar force state. This relationship indicates that the force exchanged between two material points is directed as the bond vector in the current configuration.

Ordinary elastic peridynamics materials are characterized by a scalar force state that can be derived by a potential function; specifically, the so called linear peridynamics solid scalar force state is given by (see Silling et al. (2007)):

$$\bar{t} = \frac{3K\theta}{m}\bar{\omega}\bar{x} + \alpha\bar{\omega}\bar{e}^{d} \ , \tag{3}$$

where, $\bar{x}$ is the reference position state $\bar{x} < \boldsymbol{\xi} >= \|\boldsymbol{\xi}\|$, ϑ and $\bar{e}^{d}$ are a measure of the volumetric strain and a state corresponding to the deviatoric deformation respectively (see Silling et al. (2007) for a detailed explanation of what this correspondence means). $\bar{\omega}$ is the scalar state influence function, which provides a mean to control the influence of points away from the current point on peridynamics quantities; in the present work it is equal to one. In Eq. (3) m is the weighted volume associated with the point at $\boldsymbol{x}$ (see Silling et al. (2007) for the definition), the constant K has the role of the bulk modulus, while finally the constant α is related to a corresponding shear modulus G: $\alpha = 15G/m$.

Damage can be introduced in the peridynamics equations by relatively simple means. Let the bond stretch be given by $s = \left(\|\xi + \eta\| - \|\xi\|\right) / \|\xi\|$: most damage models used in literature (e.g. by Ha and Bobaru (2010), Parks et al. (2012), Silling and Askari (2005)) assume that once a critical value of s, say s_c, is reached then the corresponding bond fails in a brittle fashion and further interaction between the corresponding material points are suppressed. Since the interactions are non-local, sudden bond failure doesn't imply the instantaneous creation of displacement discontinuity (a crack) between the two points corresponding to the failed bonds, because there can be other unbroken bonds. Failure takes place only when all the bonds intersecting some surface crossing $\mathcal{H}_x$ have failed (see the broken arrows in Figure 1). By calculating the energy required to break enough bonds within an horizon to create a fracture surface, it is possible for a given damage model to link the value of s_c to the critical strain energy release rate, e.g. Silling and Askari (2005).

As to the solution of the equations of motion (1), regardless of the actual peridynamics formulation employed, the most common strategy has been up to now based upon a "one-point quadrature" of the governing equation. The bodies to model are subdivided into volumes and the centroid of each volume is assumed to represent a material point; the only topological information required by this discretization is the connection of each material point with the points in its family. If time is itself discretized in a series of steps, the discrete form of the equations of motion for the *i*-th point at the *n*-th time step becomes (Silling and Askari (2005)):

$$\rho\ddot{\boldsymbol{u}}_i^n = \sum_p \boldsymbol{f}(\boldsymbol{u}_p^n - \boldsymbol{u}_i^n, \boldsymbol{x}_p - \boldsymbol{x}_i) V_p + \boldsymbol{b}_i^n \ , \tag{4}$$

where the summation is extended to all the points *p* in the family of point *i*. Standard techniques can be used to solve and integrate these equations over time.

3. Materials and methods

3.1. Experimental

To verify the predictive capabilities of peridynamics models with respect to mixed mode fracture, a set of experiments was performed on various specimens made of PMMA (EG 920 by LG Chemicals, South Korea). Plates were compression molded and test specimen machined to proper size.

Mode I experiments were performed on standard SEN(B) specimens following ISO 13586 prescriptions in order to determine the critical stress intensity factor (SIF) K_{IC}. Mixed-mode three point bending experiments were performed on the so called mixed-mode bending (MMB) specimens (Figure 2 (a)): these have same nominal dimensions as standard SEN(B) specimens, but the crack in this case is placed at some offset d with respect to the central load line; the larger the offset, the larger the Mode II component (see Andena et al.(2005)). For SEN(B) and MMB specimens plates with thickness *B* equal to 4 and 8 mm were used (with reference to Figure 2 (a) B is the out of plane dimension). Hence W values equal to 8 and 16 mm were selected and the span *S* was set to $4W$; two a/W ratios, 0.3 and 0.6, were tested . As to d, values between $W/2$ and $3W/2$ were used.

MMB specimens do not allow reaching large values of the ratio between the Mode II SIF, K_{II}, and the one for Mode I , K_I. Therefore asymmetric 4 point bending test (A4PB), described e.g. by He and Hutchinson (2000),

were also used (Figure 2(b)). In this work pre-cracked specimens with the following dimension were used: B =8 mm, W =16 mm b_1 = 24 mm, b_2 = 40 mm, a/W =0.3 and c values equal to 6 and 3 mm were used; in this case the shorter is c, the higher the resulting mode II component.

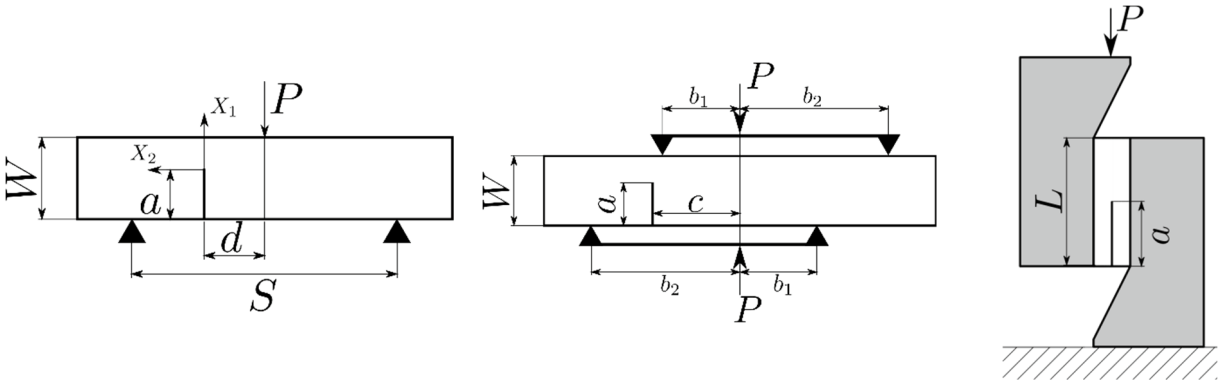

(a) (b) (c)

Figure 2. Specimen used in this work. (a) SEN(B) (if $d = 0$) and MMB. (b) A4PB. (c) CENS.

Finally, to measure pure Mode II toughness values, the so-called compact edge notch shear (CENS) specimen was used (see Caimmi et al. (2006) for a thorough description of the specimen); such a specimen, shown in Figure 2 (c) is basically a variation of classical edge-notch shear specimens. The PMMA specimen is glued with an acrylic adhesive to a steel jig, gray-filled in Figure 2 (c), which can be connected to a standard dynamometer. The load is applied via a pin on the top face of the right steel part, along the crack line. In this work specimens with L =35 mm and a/L =0.6 were used. The out of plane thickness B in this case was 10 mm.

All the test were run under crosshead displacement control at a rate of 5 mm/min. Fracture toughness was determined for all the specimens starting from the load displacement traces and following the ISO 13586 prescriptions to determine the initiation load. The shape factors used to calculate the critical SIFs were taken from Fett (2008) for the MMB specimens, from He and Hutchinson (2000) for the A4PB specimens and by running FE simulations for the CENS specimens (see Caimmi et al. (2006) for the details).

3.2. Numerical modelling

Peridynamics models of the specimens described in the previous subsections were created (Figure 3). To solve the peridynamics equations of motion (Eq.(1)) in a quasi-static setting, i.e. assuming the contribution of the inertial term to be negligible, the open source peridynamics solver Peridigm was used (Parks et al. 2012). PMMA was modelled as a linear peridynamics solid with K =3.9 GPa and G = 0.93 GPa, which were derived by the elastic modulus measured by tensile tests and by assuming a Poisson's coefficient equal to 0.33. The horizon was assumed to be δ =0.75 mm. A brittle damage model based on a critical bond stretch (Sec. 2.) was used. The value of s_c was initially estimated by the formulae valid for bond-based peridynamics formulations, provided by Silling and Askari (2005), which link s_c to the critical strain energy release rate G_{IC} and the horizon. The value was then adjusted by hand fitting in order to reproduce the fracture load recorded in SEN(B) experiments with B =4 mm; s_c was thus determined to be about 1.3 10^{-2}. This value was then used to simulate the behavior of mixed-mode and mode II specimens.

As to the discretization, if Δx is the typical grid spacing between two different discretized material points, it is necessary that the mesh resolution $r = \delta/\Delta x$ be greater than 2; values between 3 and 4 are generally chosen to balance accuracy and computational costs (Ha and Bobaru (2010)), which increase very fast with the number of neighbors in each family. In this preliminary study, a value of r equal to 3 was used almost everywhere: for example, with reference to Figure 3(a), discretization used for three point bending specimens with S =32 mm

employed a uniform grid with $r = 3$. In other cases, to limit the computational burden, in regions far away from the crack or the load points a value of $r = 2$ was used, as for example in the case of the CENS model shown in Figure 3(a). It was verified on SEN(B) specimens that these values of r are large enough to grant convergence of the predicted value of K_{IC} ; anyhow this discretization is still relatively coarse. As shown in Figure 3, 3D models of the specimens were made; however, due to symmetry, only one-half of the specimens along the thickness (z) direction was modelled. As to the boundary conditions, peridynamics requires these to be prescribed on volumes rather than on surfaces: for the three- and four-point bending tests, displacement boundary conditions were applied in the region close to the load points. The load itself was applied as a prescribed displacement boundary condition. As to the CENS specimen, to limit the computational effort, the steel jig was not modelled (i.e. it was assumed to be rigid) and the boundary conditions were applied to a layer one horizon thick at the specimen long edges: fixed displacements were prescribed on the right side and a constant velocity was prescribed on the left one. Pre-cracks (not visible in Figure 3) were created by suppressing since the beginning of the analysis interactions for bonds crossing a rectangular surface cutting through the thickness and partially through the specimen width.

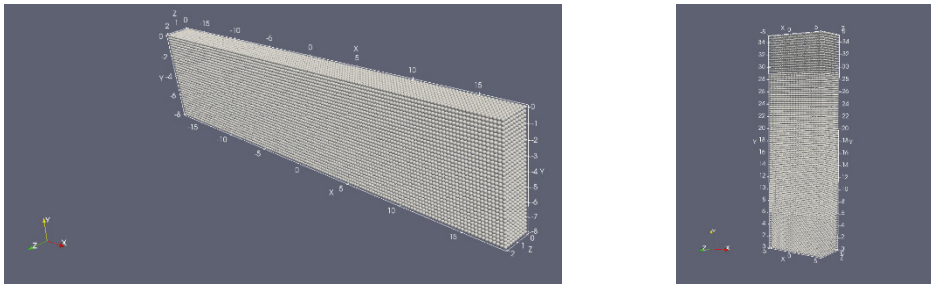

(a) (b)

Figure 3 Peridynamics discretization of the 3 point bending specimens (a) and of the CENS specimens (b).

4. Results

The main results are collected in Figure 4. In Figure 4(a) selected load displacement traces for some different bending tests are shown; the predictions from peridynamics (lines) are in line with the experimental measurements (hollow symbols) both as to the failure load and as to the initial stiffness. The experimental traces were corrected to account for the typical initial non-linear region due to indentation and plays take up. The peridynamics traces sometimes are not linear up to failure; deviations are correlated with localized damage initiation near the load points, where probably the boundary conditions are slightly too severe with respect to the mesh size used and the actual experimental loading conditions enforced by the pins; anyway the large load drops corresponding to the maximum in the load traces always corresponds to fracture initiation at the crack tip. The small differences in the initial stiffness may be explained with the relatively coarse discretization: material points lying near free boundaries experience a sort of surface tension effect as described by Mitchell et al. (2015), which can affect the global stiffness. For the CENS specimen (not shown in Figure 4(a)) a significant difference in the predicted and the measured stiffness was noted, the former being significantly stiffer; however this is probably due to the fact that the simulations neglects machine and jig stiffness, which in this case significantly contribute to the measured stiffness (see Caimmi et al. (2006)). Overall, the predictions from peridynamics display a more stable behavior than their experimental counterparts; this may due to the fact that the testing machine, with its limited stiffness, is not modelled.

To get an overall idea of the ability of the method to catch the fracture load, its critical value was determined from the simulated load-displacement traces following ISO 13586 and the procedure outlined for the experimental data in Sec.3.1 was followed to evaluate the critical SIFs; the resulting failure envelope is presented in Figure 4(b), where the circles with error bars are the experimental results, and the triangles are the corresponding peridynamics predictions. Different triangles correspond to different specimen nominal dimensions; where cluster of triangles are

present they refer to specimens which nominally should display the same mixity ratio K_{II} / K_I . Overall there is a good agreement between the measured and the predicted values, with the exception of the pure Mode II values, which are higher than the experimental ones.

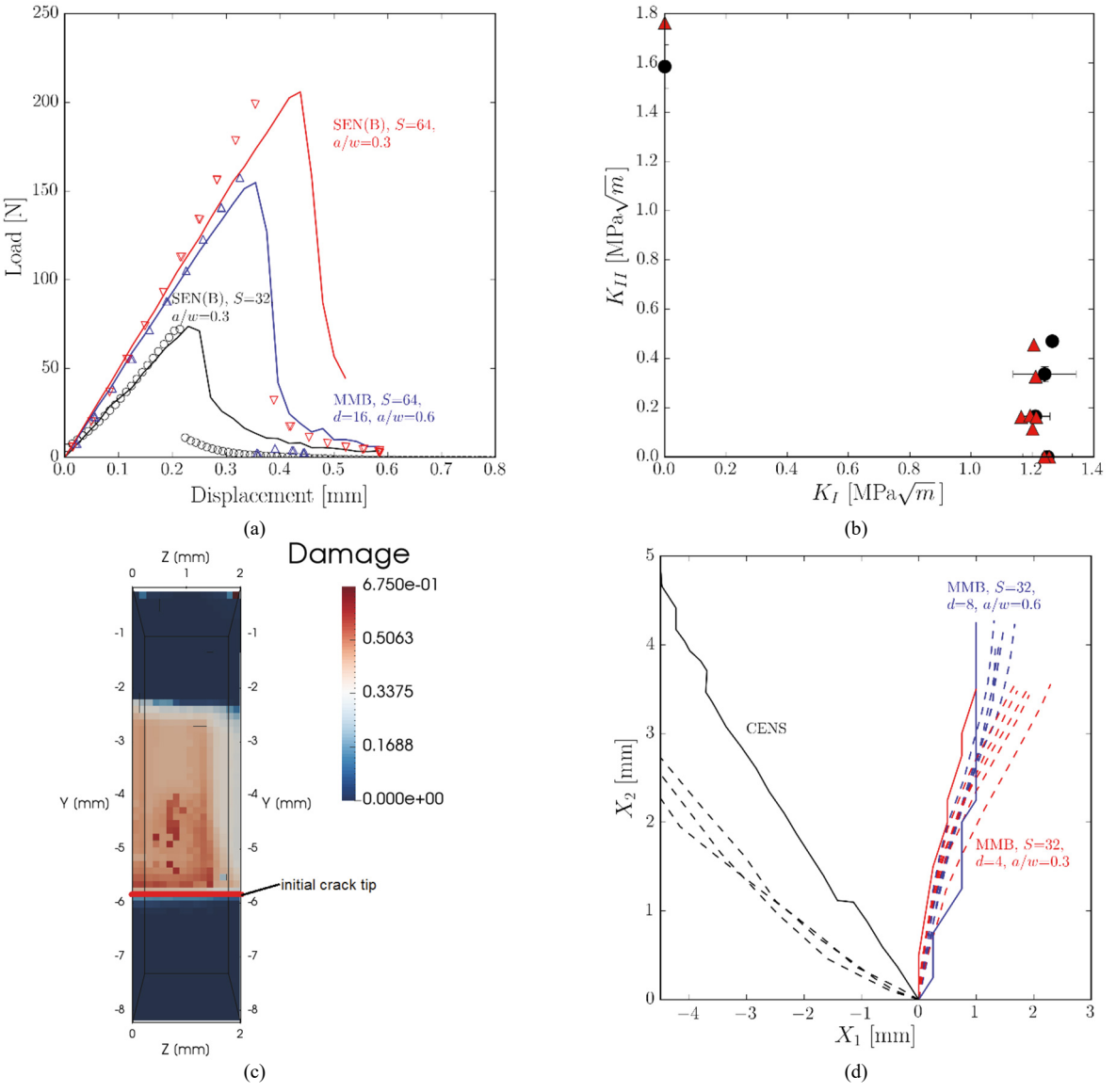

Figure 4 Peridynamics simulation results. (a) Selected experimental (symbols) and numerical (solid lines) load-displacement traces. Different colors corresponds to different samples nominal dimensions. (b) Failure envelope as obtained experimentally (dots with error bars) and numerically (triangles). (c) Crack front shape as seen perpendicularly to the crack plane for a Mode I specimen (S=32 mm, initial crack length 0.3W) after crack initiation. The picture shown corresponds to a boundary displacement of 0.27 mm. Only the z>0 half specimens is shown. Colors show the damage variables; point with damage >0.4 belong to the crack front (d) Selected crack paths for different configurations. Dashed lines are experimental values, continuous line numerical predictions. Different colors correspond to different test setups.

Figure 4(c) show for a Mode I sample with S =32 mm, W =8 mm and initial crack length a/W =0.3 the crack front after some propagation. Due to symmetry with respect to z , only the half of the specimen with z >0 is shown. The colors represents the standard damage variable used in peridynamics (see Ha and Bobaru (2010) for the precise definition). Broadly speaking, a value of the damage variable greater than about 0.4 for a given material

point means that a crack completely crosses its family. As it can be seen, the crack front correctly shows the nail shape typical of brittle fracture, at least in a qualitative sense.

As to the crack paths, these were measured on the free surface of the tested samples and compared in Figure 4(d) (dashed lines) with those obtained from the simulations (continuous lines) for some of the tested samples. Crack paths are represented in a reference system centered at the initial crack tip in the undeformed configuration (see Figure 2 (a)). For the MMB specimens shown, there is a qualitative agreement between the predicted and the measured paths, although some differences are there. In particular, for the case with d=4 there is a very good agreement with the exception of small deviation after some propagation occurred; anyhow the slope seems correct. As to the case d=8 the overall trend is captured but in very rough way; a finer discretization might have provided better results. This is also possibly true for the CENS specimens where the initial propagation angle, which experimentally is about 70°, a value consistent with most theoretical propagation criteria, could not be captured by the simulations; they can anyhow fairly reproduce the slope of the propagation path, which is about 45°, again consistently with the theoretical predictions.

5. Summary and Conclusions

Peridynamics was used to simulate fracture in different laboratory specimens. A simple brittle linear peridynamics elastic material was used to model PMMA; the critical bond stretch was determined by fitting the results to SEN(B) specimens and used to predict the behavior of the other tests. Good results were obtained as to the fracture toughness, with the exception of pure Mode II values which were overestimated. The one-parameter fracture criterion was also shown to provide a qualitative agreement as to the predictions of crack path in a three dimensional setting; possible improvements might be obtained with finer discretizations.

References

Andena, L., A. Corigliano, R. Frassine, S. Mariani 2005. Mixed-mode crack growth in toughened PMMA. 11th International Conference on Fracture. Turin, IT, 20-25 March.

Agwai, A., I. Guven, E. Madenci 2008. Peridynamic theory for failure prediction in multilayer thin-film structures of electronic packages. Electronic Components and Technology Conference (ECTC) 2008, 27-30 May, Lake Buena Vista, FL, US:1614 - 1619

Ayatollahi M.R., Aliha M.R.M. 2009 Analysis of a new specimen for mixed mode fracture tests on brittle materials. Engineering Fracture Mechanics 76:1563–1573

Caimmi, F., R. Frassine, A. Pavan 2006. A new jig for mode II interlaminar fracture testing of composite materials under quasi-static and moderately high rates of loading. Engineering Fracture Mechanics 73 (16): 2277- 2291.

Fett, T. 2008. Stress Intensity Factors –T-Stresses –Weight Functions. Universitätsverlag Karlsruhe, Karlsruhe, D.

Foster, J. T., S. A. Silling, W. W. Chen 2010. Viscoplasticity using peridynamics. International Journal for Numerical Methods in Engineering 81 (10): 1242-1258.

Ha, Y. D., F. Bobaru 2010. Studies of dynamic crack propagation and crack branching with peridynamics. International Journal of Fracture 16 (1-2): 229-244.

He, M., J. Hutchinson 2000. Asymmetric four-point crack specimen. Journal of applied mechanics 67 (1): 207-209

Madenci, E., E. Oterkus 2013. Peridynamic theory and its Applications. Springer Verlag, New York, US.

Mitchell, J. A, 2011. A nonlocal, ordinary, state-based plasticity model for peridynamics.Techinical Report SAND2011-3166, Sandia National Laboratories.

Mitchell, J., S. A. Silling, D. J. Littlewood, 2015. A position-aware linear solid constitutive model for peridynamics. Journal of Mechanics of Materials and Structures 10 (5): 539-557.

Oterkus, E., E. Madenci, 2012. Peridynamic analysis of fiber-reinforced composite materials. Journal of Mechanics of Materials and Structures 7 (1): 45-84.

Oterkus, S., J. Fox, E. Madenci 2013. Simulation of electro-migration through peridynamics, IEEE 63rd electronic components and technology conference (ECTC), New York, USA.

Parks M.L., D.J. Littlewood, J.A. Mitchell,S.A. Silling, 2012. Peridigm users' guide, Techincal Report SAND2012-7800, Sandia National Laboratories.

Silling S.A, 2000 , Reformulation of elasticity theory for discontinuities and long-range forces. Journal of the Mechanics and Physics of Solids 48, 175-209

Silling, S. A., E. Askari 2005. A meshfree method based on the peridynamic model of solid mechanics. Computers & Structures 83(17–18): 1526-1535.

Silling S. A., M. Epton, O. Weckner, J. Xu, E. Askari, 2007. Peridynamic States and Constitutive Modeling. Journal of Elasticity 88 (2): 151-184.